Novel Topology of Reversed Wave Attenuation in Microstrip Ferrite Edge-Guided Mode Isolator

Sokha Khim, Thierry Monediere, Hervé Parvery, Bouchra Frigui, Damien Passerieux, Jehison Leon Valdes, and Laure Huitema, *Member, IEEE*

***Abstract*—This letter reports a novel ferrite isolator topology based on the edge-guided mode principle with an asymmetrical stub perturbation that achieves nonreciprocal behavior without absorbers, shorted strips, or vias. Implemented on a single metallized ferrite substrate, the design offers a clean, low-cost, and highly reproducible solution compatible with planar fabrication processes. Unlike prior edge-guided mode implementations, the proposed topology enables reverse-wave suppression using only geometrical perturbations, significantly simplifying fabrication and improving integrability. A prototype operating at 2.4 GHz was designed using combined electromagnetic (EM)–magnetostatic (MS) simulations and then fabricated for experimental validation. Measurements confirm a worst case insertion loss of 1.5 dB and a 6.6% fractional bandwidth where both reflection and isolation exceed 20 dB. The compact, via-free structure and its compatibility with planar antennas make this isolator a suitable building block for front-end modules in wireless communication systems, particularly where size and manufacturability constraints dominate.**

***Index Terms*—Edge-guided mode isolator, ferrite, field displacement, isolator, nonreciprocal device.**

I. Introduction

NONRECIPROCAL devices such as isolators and circulators are indispensable in modern microwave systems, ensuring stability and reliability in applications from wireless networks to radar and satellite communications [1], [2], [3]. Achieving compact, integrable, and low-cost ferrite-based solutions remains a longstanding challenge, as most conventional implementations rely on bulky loads and connectorized devices [4], [5], [6]. Moreover, these configurations make integration challenging and limit device performance.

The edge-guided mode isolator, pioneered by Hines [7], offers a more integrable alternative by exploiting asymmetric field displacement in magnetized ferrite microstrip lines. However, nonreciprocal hinges on lossy absorbers are placed on one side of an identical edge mode. Recent works that embodied Hines's principle have emerged [8], [9], [10], [11], [12], [13]. Despite good performance, most realizations of this principle still depend on lossy absorbers, short-circuited strip terminations, and complex fabrication steps, which complicate reproducibility and scalability. As a result, there is still no widely adopted approach that combines design simplicity, fabrication ease, and high performance, leaving a clear opportunity for further innovation.

It has been demonstrated that a miniaturized planar isolator with isolation greater than 20 dB can be achieved using a single open stub based on the edge-guided mode principle [13]. The remaining losses and mismatches are mainly due to magnetic losses in the ferrite and limitations related to the stub configuration and placement.

This work addresses these challenges by introducing a new isolator topology that replaces absorbers, vias, short-circuited strips, and external matched loads with a purely geometrical perturbation strategy based on asymmetrical stubs. This approach represents a significant departure from conventional edge-guided mode isolators, offering a simpler, cleaner, and highly integrable design compatible with standard PCB processes. By carefully selecting the ferrite material parameters and optimizing the asymmetrical stub configuration, the proposed device achieves strong nonreciprocity while maintaining compactness, reproducibility, and low insertion loss. Operating in the 2.4–2.5-GHz ISM band, the required bandwidth is naturally accommodated by the device, whose fractional bandwidth is governed by the combined choice of ferrite saturation magnetization and internal magnetic field, which together define the frequency band where the effective permeability becomes negative, which is the operating region of an edge-guided mode isolator. Furthermore, the simplicity of this topology directly facilitates its integration into compact front-end architectures, including ferrite-loaded antennas operating in the negative-effective-permeability region [14], enabling application-driven codesign opportunities.

II. Design Principle of Edge-Guided Mode Isolator

Ferrite is usually characterized by a permeability tensor. It describes their nonreciprocal behavior when they are biased by a continuous (dc) magnetic field. When the dc magnetic field is strong enough to saturate the ferrite, its permeability tensor is described by the following equation called the Polder tensor [2], [15]:

$$[\mu_r(\omega)] = \begin{bmatrix} \mu & -j\kappa & 0 \\ j\kappa & \mu & 0 \\ 0 & 0 & 1 \end{bmatrix} \quad (1)$$

Received 10 September 2025; revised 3 December 2025; accepted 31 December 2025. Date of publication 15 January 2026; date of current version 11 May 2026. This work was supported by the L'Agence de l'Innovation de la Défense (AID) et l'Agence Nationale de la Recherche (ANR) as part of the Co-integration of a compact, high-performance isolator and Antenna through development of a dedicated self-polarized FErrite substrate (CAFE) Project under Grant ANR-24-ASTR-0019. *(Corresponding author: Sokha Khim.)*

Sokha Khim is with CISTEME, 87280 Limoges, France, and also with XLIM, UMR CNRS 7252, University of Limoges, 87060 Limoges, France (e-mail: sokha.khim@unilim.fr).

Thierry Monediere, Damien Passerieux, and Jehison Leon Valdes are with XLIM, UMR CNRS 7252, University of Limoges, 87060 Limoges, France (e-mail: thierry.monediere@unilim.fr; damien.passerieux@xlim.fr; jehison.leon-valdes@unilim.fr).

Hervé Parvery and Bouchra Frigui are with CISTEME, 87280 Limoges, France (e-mail: parvery@cisteme.net; frigui@cisteme.net).

Laure Huitema is with XLIM, UMR CNRS 7252, University of Limoges, 87060 Limoges, France, and also with the Institut Universitaire de France (IUF), 75005 Paris, France (e-mail: laure.huitema@unilim.fr).

Digital Object Identifier 10.1109/LMWT.2026.3651400

2771-957X © 2026 IEEE. All rights reserved, including rights for text and data mining, and training of artificial intelligence and similar technologies. Personal use is permitted, but republication/redistribution requires IEEE permission.
See https://www.ieee.org/publications/rights/index.html for more information.

Authorized licensed use limited to: Universite De Limoges. Downloaded on October 01,2026 at 11:09:08 UTC from IEEE Xplore. Restrictions apply.

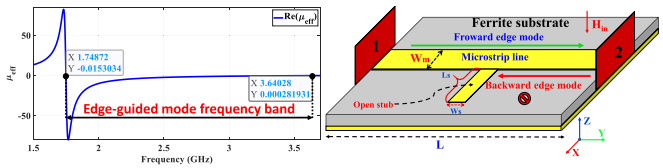

(a) (b)

Fig. 1. (a) Real part of μ_{eff} versus frequency for a Y210 ferrite ($4\pi Ms$ = 1000 G, ε_r = 14.2, ΔH = 10 Oe, and H_{in} = 300 Oe). (b) Edge-guided mode isolator with single stub (L = 12 mm, W_m = 5.5 mm, L_s = 12.2 mm, and W_s = 0.2 mm).

where the elements of the permeability tensor are given by the following equation:

$$\mu = 1 + \frac{\omega_m \omega_0}{\omega_0^2 - \omega^2} = \mu' - j\mu''$$
$$\kappa = \frac{\omega_m \omega}{\omega_0^2 - \omega^2} = \kappa' - j\kappa'' \tag{2}$$

where $\omega = 2\pi f$ is the angular microwave frequency, $\omega_m = \gamma\mu_0 M_s$ is the gyrotropic frequency, $\omega_0 = \gamma\mu_0 H_{\text{in}} + j\omega\alpha$ is the Larmor frequency, and γ = 2.8 MHz/Oe is the gyromagnetic ratio. α is the damping factor that determines the magnetic losses of ω_0. The permeability tensor elements are proportional to the internal magnetic field (H_{in}) and the saturation magnetization ($4\pi M_s$). In addition, magnetic losses are modeled by the damping factor $\alpha = \gamma\Delta H/2f$, where ΔH is the ferrite resonance linewidth and f is the microwave frequency. Another key parameter in determining the operational behavior of ferrite-based devices is the effective permeability, defined as follows, where μ and κ are calculated from (2):

$$\mu_{\text{eff}} = \frac{\mu^2 - \kappa^2}{\mu}. \tag{3}$$

The plot of the real part of the effective permeability for commercial ferrite Y210 from Exxelia under an internal field of 300 Oe is shown in Fig. 1(a). It reveals that the effective permeability μ_{eff} exhibits a resonance and becomes negative between 1.75 and 3.6 GHz. In this region, a field displacement phenomenon occurs, enabling the design of an edge-guided mode isolator [7], [9].

Prior references have attempted to suppress backward waves based on resistive sheets/lossy absorbers, matched loads, or short-circuited strips, but these complicate integrations and make reproducibility difficult. This work adopts a simpler solution: open-circuit stubs that generate nonreciprocal behavior on a single ferrite substrate. This method, whose concept is illustrated in Fig. 1(b), is novel and excludes traditional approaches while offering a clean, low-cost, and integrable topology.

III. Asymmetrical Serrated Topology and Isolation

A lateral open-circuit stub on a ferrite substrate with an internal magnetic bias (300 Oe) was used to demonstrate nonreciprocity. Positioned asymmetrically, the stub absorbed signals returning from port 2, yielding 2-dB isolation and good matching near 2.4 GHz, while the forward waves experienced low insertion loss. To improve isolation without affecting forward transmission, multiple stubs were added in an asymmetric serrated structure, enhancing backward absorption. A parametric analysis of this design is presented in Fig. 2.

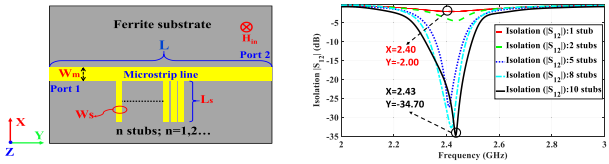

(a) (b)

Fig. 2. (a) Schematic of isolator with evolution of stub from 1 to 10 (L = 12 mm, W_m = 5.5 mm, L_s = 12.2 mm, W_s = 0.2 mm, and a gap of 0.1 mm). (b) Evolution of S-parameters as the stub increases from 1 to 10.

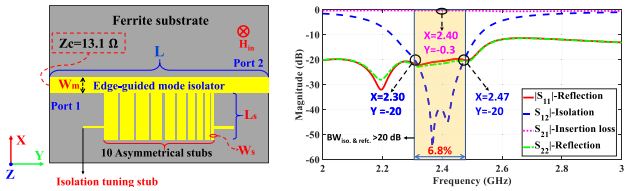

(a) (b)

Fig. 3. (a) Schematic of an isolator with asymmetrical stubs; W_s = 0.2–0.92 mm the first stub width W_1 = 0.2 mm; $W_2 = W_1 + a$ with a = 0.08 mm; and so on. The width of the isolation tuning stub equals 0.1 mm. (b) S-parameters' performance.

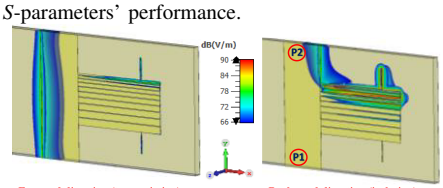

(a) (b)

Fig. 4. Electric field at 2.40 GHz in (a) forward and (b) backward directions.

Fig. 2 shows that implementing ten identical stubs achieves over 30 dB of isolation, meeting industrial requirements. Although a linear array of identical stubs significantly improves isolation, further enhancement is possible by introducing asymmetry into the stub geometry. Varying the stub widths modifies their inductive properties, forming a distributed reactive network that enables broader absorption. At this stage, interstub coupling is carefully controlled through precise spatial placement and optimization of stub dimensions and spacing, performed with full-wave computer simulation technology (CST). This approach ensures a balance between isolation and reflection coefficients better than 20 dB. Further refinement is achieved by inserting small isolation-tuning stubs into the asymmetrical configuration [see Fig. 3(a)]. These additional stubs provide fine-tuning flexibility, improving the balance of isolation and reflection around 2.4 GHz, as shown in Fig. 3(b). The design maintains excellent forward insertion loss, while reflections ($|S_{11}|$, $|S_{22}|$) and isolation ($|S_{12}|$) remain below 20 dB across a fractional bandwidth of 6.8% centered at 2.4 GHz.

In addition, Fig. 4 presents the electric field distributions captured at 2.40 GHz. Fig. 4(a) illustrates edge-guided in forward propagation with minimal insertion loss, while Fig. 4(b) confirms the complete absorption of the backward wave, achieving a peak isolation ($|S_{12}|$) of 55 dB [see Fig. 3(b)].

IV. EM–MS Simulations and Validation

Up to this point, the isolator analysis has been performed under idealized conditions, with excitation ports normalized to the characteristic impedance of the transmission line. For practical integration into a 50-Ω system, however, proper

Authorized licensed use limited to: Universite De Limoges. Downloaded on October 01,2026 at 11:09:08 UTC from IEEE Xplore. Restrictions apply.

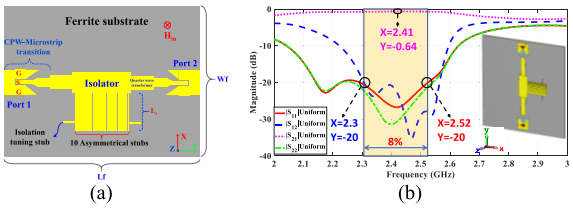

(a) (b)

Fig. 5. (a) Top view of the isolator with impedance matching and transition to coplanar: ($L_f \times W_f \times h = 50 \times 50 \times 1$ mm). (b) S-parameter of $H_{in} = 300$ Oe.

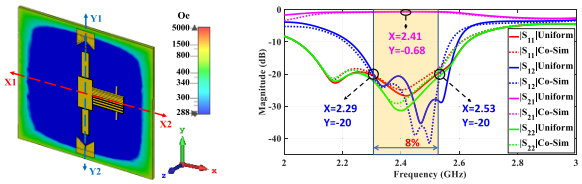

(a) (b)

Fig. 6. (a) Inhomogeneous field inside ferrite using a SmCo5-18MGO magnet. (b) Comparison of uniform field (solid lines) and cosimulation (dotted lines).

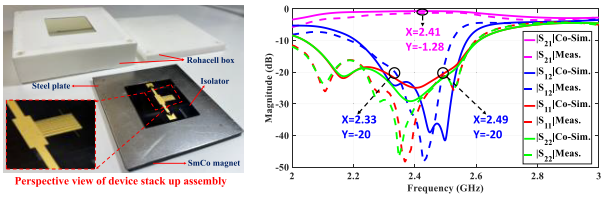

(a) (b)

Fig. 7. (a) Prototype of the isolator. (b) Simulated (solid lines) and measured performances (dashed lines) of the proposed edge-guided mode isolator.

impedance-matching transitions are necessary to preserve device performance.

Fig. 5(a) shows the complete isolator model, including the impedance transformer, as well as the ground–signal–ground (GSG)-compatible pads and transitions required for on-wafer measurements. The transition and impedance matching were independently optimized prior to integration with the isolator.

Electromagnetic (EM) simulations were initially carried out under a uniform bias field of 300 Oe, ensuring operation within the band of the negative effective permeability required for edge-guided modes [see Fig. 5(b)]. To evaluate practical conditions, EM–magnetostatic (MS) cosimulations were conducted with an inhomogeneous biasing distribution, as illustrated in Fig. 6(a). The resulting performance, compared with the homogeneous bias case in Fig. 6(b), shows only slight variations in isolation magnitude and reflection characteristics under realistic magnetic biasing, confirming that the magnet beneath the device was properly dimensioned. Indeed, the isolator maintains a fractional bandwidth of about 8% with at least 20-dB isolation, and exhibits ($|S_{21}|$) of only 0.68 dB at 2.41 GHz.

To validate the concept, the isolator was fabricated on a polished ferrite substrate ($50 \times 50 \times 1$ mm^3). A metallic seed layer (Ti/Au, 40/400 nm) was first deposited by E-beam evaporation, followed by gold electroplating to reach a total thickness of 15 μm. The circuit pattern on the top surface was defined using an LPKF ProtoLaser U4, while the backside was fully metallized to serve as the ground plane. Magnetic bias was provided by an external samarium–cobalt permanent magnet with steel plates to enhance field uniformity. The assembly was enclosed in a low-permittivity Rohacell box ($\varepsilon_r \approx 1$) for probe access and mechanical support, as shown in Fig. 7(a).

TABLE I
COMPARISON WITH SIMILAR WORKS

Ref.	Year	Percentage BW (%)		*|S21| (dB)	Approach	×Int.	¨Comp.	(L x W) in term of (λ_0) at F_c
		‖BW$_{r\&i}$	‖BW$_i$					
[12]	2007	0	11.7	10	Shorted strips	Yes	Medium	$(0.3\times0.1)\lambda_0$
[11]	2014	0	23	5	Shorted strips	Yes	Medium	$(1.2\times0.3)\lambda_0$
[9]	2018	4.8	32	2.9	Shorted strips	No	Medium	$(0.8\times0.4)\lambda_0$
[16]	2021	0	10	1	Terminated load	Yes	Medium	$(0.9\times0.5)\lambda_0$
[10]	2021	1.7	5.3	3	Resonance absorption	No	High	$(4.7\times0.5)\lambda_0$
[8]	2023	112	112	1	Absorber	No	High	$(1.4\times1.1)\lambda_0$
[17]	2024	0	3.4	2.29	Terminated load	Yes	Medium	$(0.2\times0.2)\lambda_0$
T.W	2025	6.6	6.6	1.5	**Asymmetrical stubs**	Yes	Low	$(0.4\times0.4)\lambda_0$

‖BW$_{r\&i}$=BW of $|S_{11}|$;$|S_{22}|$&$|S_{12}|$>20 dB;‖BW$_i$=BW of $|S_{12}|$>20 dB; ×Int.=Integration possibility;¨Comp.=Complexity of fabrication;*$|S_{21}|$=At max.

The measured S-parameters of the device are presented in Fig. 7(b). The experimental data exhibit a good agreement with the simulation results, with amplitude and bandwidth variations within ±2.5%. The maximum measured isolation ($|S_{12}|$) reaches 48.40 dB at 2.42 GHz. Reflection coefficients ($|S_{11}|$) and ($|S_{22}|$), as well as the isolation, remain below 20 dB over the frequency range from 2.33 to 2.49 GHz, corresponding to a relative bandwidth of 6.6%. The measured minimum insertion loss ($|S_{21}|$) in the working band is 1.28 dB. The slight enhancements in isolation ($|S_{12}|$) and reflections ($|S_{22}|$), compared to simulations, are attributed to fabrication tolerances (e.g., coplanar line and stub widths) and minor variations in the internal magnetic bias field under the permanent magnet. Table I provides a comparative summary with other state of the art based on edge-guided and alternative nonreciprocal mechanisms. The key comparison metric is the fractional bandwidth (BW$_{r\&i}$), defined under a stringent criterion: the frequency range over which both reflection coefficients ($|S_{11}|$, $|S_{22}|$) and isolation ($|S_{12}|$) remain better than 20 dB. Additional columns, including year of publication, perturbation strategy, devices' dimensions, and so on, are also considered.

Compared with prior works, the proposed design exhibits the following key advantages and limitations.

1) Reverse-wave suppression is achieved using novel asymmetrical stubs, without the need for absorbers, shorted strips, or external loads used as in [8], [9], [11], and [16], while still achieving stringent BW$_{r\&i}$ > 20 dB.

2) Compact, low-cost, highly reproducible, and easily manufacturable topology on a single-layer PCB-compatible substrate, offering advantages over [8], [9], [10].

3) Maximum insertion loss of 1.5 dB, outperforming [9], [10], [11], [12], [17], though not suitable for ultralow-loss applications such as in [8] and [16].

4) Fractional bandwidth of 6.6%, which limits suitability for wideband systems such as those reported in [8].

5) requires external magnetic biasing, unlike the ultracompact self-biased W-band isolator reported in [17].

V. CONCLUSION

This work has demonstrated that asymmetrical stub perturbations in an edge-guided ferrite structure provide a simple alternative to absorbers, vias, shorted strips, and external loads for achieving nonreciprocity. Implemented on a single metallized ferrite substrate, the proposed design improves manufacturability, reproducibility, and ease of integration within planar microwave circuits. A fabricated prototype validated through EM–MS cosimulations and measurements

Authorized licensed use limited to: Universite De Limoges. Downloaded on October 01,2026 at 11:09:08 UTC from IEEE Xplore. Restrictions apply.

achieved a worst case insertion loss of 1.5 dB with an isolation greater than 20 dB across a 6.6% bandwidth at 2.41 GHz.

Beyond its intrinsic performance, the via- and absorber-free architecture naturally supports cofabrication with antennas or other passive components on the same substrate. This makes the isolator a strong candidate for compact, magnetically biased front-end modules, including antenna–isolator integrated structures for ISM-band communication systems.

ACKNOWLEDGMENT

This work was carried out at the INOGYRO joint laboratory between the SME Inoveos and the XLIM Research Institute (https://inogyro.xlim.fr/). The circuit etching was carried out at Inoveos (LPKF ProtoLaser U4). All or part of the experiments were carried out at the PLATINOM test platform at XLIM, a member of the CNRS RF-Net network.

REFERENCES

[1] D. M. Pozar, *Microwave Engineering*, 4th ed., Hoboken, NJ, USA: Wiley, 2011.

[2] J. D. Adam, L. E. Davis, G. F. Dionne, E. F. Schloemann, and S. N. Stitzer, "Ferrite devices and materials," *IEEE Trans. Microw. Theory Techn.*, vol. 50, no. 3, pp. 721–737, Mar. 2002, doi: 10.1109/22.989957.

[3] V. G. Harris, *Modern Ferrites, Volume 2: Emerging Technologies and Applications*, vol. 2. Hoboken, NJ, USA: Wiley, 2022.

[4] S. Khim, S. Cheab, S. Soeung, and G. S. Ng, "Design and synthesis of ferrite strip-line circulator based on enhanced closed form solution and power handling analysis," *IEEE Access*, vol. 10, pp. 112812–112831, 2022.

[5] L. Marzall, D. Psychogiou, and Z. Popovic, "Microstrip ferrite circulator design with control of magnetization distribution," *IEEE Trans. Microw. Theory Techn.*, vol. 69, no. 2, pp. 1217–1226, Feb. 2021, doi: 10.1109/TMTT.2020.3045995.

[6] V. Olivier et al., "General coupling method for stripline ferrite circulators: Application on dual-band devices with complex central conductor shape," *IEEE Trans. Microw. Theory Techn.*, vol. 70, no. 7, pp. 3486–3497, Jul. 2022, doi: 10.1109/TMTT.2022.3175168.

[7] M. E. Hines, "Reciprocal and nonreciprocal modes of propagation in ferrite stripline and microstrip devices," *IEEE Trans. Microw. Theory Techn.*, vol. MTT-19, no. 5, pp. 442–451, May 1971.

[8] L. Zeng, C.-Y.-E. Tong, and S. N. Paine, "A low-insertion loss cryogenic edge-mode isolator with 18 GHz bandwidth," *IEEE J. Microw.*, vol. 3, no. 4, pp. 1258–1266, Oct. 2023, doi: 10.1109/JMW.2023.3307297.

[9] W. Marynowski, "Integrated broadband edge-guided mode isolator with antiparallel biasing of the ferrite slabs," *IEEE Microw. Wireless Compon. Lett.*, vol. 28, no. 5, pp. 392–394, May 2018.

[10] M. Noferesti and T. Djerafi, "A tunable ferrite isolator for 30 GHz millimeter-wave applications," *IEEE Trans. Magn.*, vol. 57, no. 7, pp. 1–7, Jul. 2021.

[11] M. F. Farooqui, A. Nafe, and A. Shamim, "Inkjet printed ferrite-filled rectangular waveguide X-band isolator," in *IEEE MTT-S Int. Microw. Symp. Dig.*, Jun. 2014, pp. 1–4.

[12] T. Ueda and M. Tsutsumi, "Nonreciprocal left-handed transmission characteristics of microstriplines on ferrite substrate," *IET Microw., Antennas Propag.*, vol. 1, no. 2, pp. 349–354, Apr. 2007, doi: 10.1049/iet-map:20050006.

[13] S. Khim, J. L. Valdes, H. Parvery, L. Huitema, and T. Monediere, "Planar isolator based on field displacement in ferrite substrate," in *Proc. 54th Eur. Microw. Conf. (EuMC)*, Sep. 2024, pp. 172–175, doi: 10.23919/EuMC61614.2024.10732277.

[14] J. Leon Valdes, T. Monédière, E. Arnaud, S. Jemmeli, and L. Huitema, "Multiband circularly polarized ferrite antenna operating with negative effective permeability," *IEEE Trans. Antennas Propag.*, vol. 73, no. 12, pp. 9710–9720, Dec. 2025, doi: 10.1109/TAP.2025.3611684.

[15] B. Laxand K. J. Button, *Microwave Ferrites and Ferrimagnetics*. New York, NY, USA: McGraw-Hill, 1962.

[16] V. Laur, J. P. Gouavogui, and B. Balde, "C-band hybrid 3-D-printed microwave isolator," *IEEE Trans. Microw. Theory Techn.*, vol. 69, no. 3, pp. 1579–1585, Mar. 2021, doi: 10.1109/TMTT.2021.3053277.

[17] E. Roue. (Oct.2024). *Towards W-Band Self-Biased Circulators for Next Generation of VHTS Payload*. [Online]. Available: https://www.spcd.space/past-events.php

Authorized licensed use limited to: Universite De Limoges. Downloaded on October 01,2026 at 11:09:08 UTC from IEEE Xplore. Restrictions apply.